

An Analytical Model for Explosive Compaction of Powder to Cylindrical Billets through Axial Detonation

B. Srivathsa¹ and N. Ramakrishnan²

Abstract: An analytical model, describing an explosive compaction process performed axially on a powder assembly of cylindrical geometry, is discussed. The powder is encapsulated in a cylindrical metal container surrounded by an explosive pad, which is detonated parallel to the major axis of the compact. The pressure generated in the powder is a function of the nature and the thickness of the explosive material as well as the powder characteristics. The model is based on the principle of shock propagation in powder aggregate and, the detonation as well as the refraction wave characteristics of the explosives. For the purpose of validation and illustration, this investigation considers the explosive compaction of aluminium powder particles for different explosive pad thicknesses. The model brings-out a closed-form solution for densification of powders. The density of the final powder compact depends on the pad thickness. Inadequate pad thickness leads to under compacted core, while higher pad thickness leads to melting at the core leading to over all low density. The optimum pad thickness of the explosive to produce the highest densification is thus determined using the model. The densification depends on the size of the powder particles also, since; the heat generated by the high pressure shock wave melts the surface of the powder particles depending on the specific heat, thermal conductivity and the latent heat of the powder material. The study essentially covers the effect of the explosive pad thickness and the particle size of the powder on densification. The analytical results are compared with a few experimental data

and the comparison is found to be satisfactory.

Keyword: Explosive compaction, Shock wave propagation, and densification of powder.

Nomenclature

a	sound speed in the gaseous state of explosive
a_j	sound speed in the Chapman-Jouguet state
c_v	specific heat at constant volume of the material
b_k	constant appearing in Equation (5)
g_0	material parameter in a dense medium (for zero porosity)
g_θ	material parameter in a porous medium (for porosity θ)
k	thermal conductivity of the material
r	radius of the powder particle
t	time taken by the shock wave to travel through one powder particle
u_f	final particle velocity
u_i	initial particle velocity
C_0	sound speed in the powder material (for zero porosity)
C_θ	effective bulk sound speed (for porosity θ)
E_f	final internal energy after the passage of the shock wave
E_i	initial internal energy before the passage of the shock wave
K_0	bulk modulus of the material (for zero porosity)
L	Latent heat of the powder material
P_f	final pressure
P_i	initial pressure
P_j	Chapman-Jouguet pressure
T_f	final temperature of the material
T_m	melting or softening temperature of the material
T_r	room temperature

¹Computer Modelling and Simulation Group, Defence Metallurgical Research Laboratory, Hyderabad – 500 058, India, bsv@indiainfo.com, srivathsa_boddapati@rediffmail.com

²Regional Research Laboratory, Bhopal- 462 026, India, ramkrish@sify.com

U	shock velocity in dense material
U_θ	shock velocity in the porous material (for porosity θ)
V_0	specific volume of the dense solid
V_f	final specific volume
V_i	initial specific volume
V_θ	volume of the pores per unit mass (for porosity θ)
α	a fraction less than one used in Equation (18)
γ	adiabatic coefficient (gaseous state of explosive)
η	the energy deposited on the particle surface given by Equation (10)
ν	Poisson's ratio
θ_f	final porosity
θ	porosity at any instant
ρ_0	density of the powder material (for zero porosity)
ρ_e	density of the explosive
ρ_{sf}	final density of the powder due to shock loading
ρ_{si}	initial density of the powder due to shock loading
ρ_{tf}	final density of the powder due to thermal loading
ρ_{ti}	initial density of the powder due to thermal loading
ρ_j	Chapman-Jouguet density
ψ	pore collapse function used in Equation (5)
ω	thickness of the surface layer through which deposited heat energy is conducted
ω^*	thickness of the surface layer which gets melted by the energy deposition
$\Delta\rho$	increase in density due to surface melting
ΔV_θ	melted surface volume that fills the pores per unit mass
ΔV	change of volume due to sock loading per unit mass

1 Introduction

Explosive compaction of powder has emerged as an important technique and preferred to conventional ones in certain cases where (i) powders cannot be compacted through conventional routes due to their high strength and (ii) post compaction

sintering has a deteriorating effect on the mechanical properties and the desired shapes. In explosive compaction, densification of powder is achieved by a high-pressure shock wave induced by an explosive. Although, densification of powder is mainly due to the deformation of the particles during the shock loading, the surface melting caused by the heat generated by the particle deformation also contributes significantly to the densification (James, 1972; Prummer RA, 1972; LLNL report, 1981; NMAB report, 1983; Gohl WB, 2000).

Models for shock densification have been proposed in the past based on shock induced particle deformation (Bergmann OR, 1965, Carlson RJ, 1966; Grover R, 1974; Lennon CRA, 1978; Raybould D, 1981; Lee YK, 1985; Rajendran AM, 2002; Liu HT, 2006) as well as energy deposition on the surface of the particle causing melting (Bogdanov, 1969; Raybould D 1980; Gourdin, 1984; Schwartz RB 1984; Maksimenko LA, 1991; Byvshikh AI, 1991; Benson, 1994; Prummer, 2004). Yukio Sano (1977) suggested a model based on continuum approach assuming the powder to be in a compressed state under a plane shock wave. Jump conditions, representing the conservation equations, are used to calculate the density of the compacts. He specially discussed the effect of velocity on the density of the compacts. Lotrich et al (1986) proposed a one-dimensional model to describe the inhomogeneous temperature distribution in dynamically compacted powders. The model considered the effect of shock compression of the gas in the voids upon pore collapse on the thermal deposition. Raybould (1980) suggested an empirical model using discrete shock wave approach and calculated compact density and over-all temperature rise. He assumed the heat deposition to take place instantaneously on the surface of the spherical particles when the shock wave passes through a particle. Schwarz et al (1984) analysed the temperature kinetics pertain to shock consolidation of powder particles of various sizes. The model is based on heat deposition, and the time scales were calculated for the consolidation of the powder particles. This model provides an upper bound

to the melt fraction of the powder particles and the rise in temperature at the surface as a function of particle size. Gourdin (1984) described a model for the deposition of heat at powder particle surfaces during compaction. The average energy flux incident on the surface of a powder particle is estimated to be a fraction (about 90%) of the specific energy and this flux is assumed to be constant over the time taken for the shock wave to cross one powder particle. Local temperature distribution during compaction of various powders like steel, aluminium, and copper is also discussed. He noticed that the surface temperature increases with particle size. Roshan Kumar et al (1999) carried-out FEM simulation studies on dynamic compaction of metal powders. This study employs micro-mechanics of inter particle friction to discuss surface temperature rise. Shujie et al (1994) described a semi-empirical compaction equation for powder materials, which describes the relationship between the green density of compacts and applied external pressure.

In this paper, we present a model taking the shock induced particle deformation as well as surface melting due to the shock energy deposition. The model is based on conservation equations of shock propagation in porous materials (Ramakrishnan, 1988) and also due to surface melting similar to that presented by Gourdin (1984). We consider a typical cylindrical geometry as shown in Figure 1. The model describes the temperature rise during compaction and the particle surface melt zone and relates them to the initial particle size of the powder. Although, this model is similar to the model described by the earlier researcher (Raybould, 1980), this work presents a closed form solution for densification due to shock loading as well as melting of the powder surface layer. Combining the densification due to loading as well as melting makes the model comprehensive and realistic. Densification variation in spatial as well as temporal scales can be computed using the model. These results are validated with the published results for shock consolidation pertaining to the effect of particle size and also densification due to melting into account.

2 Densification due to shock induced deformation

The model assumes that the powder encapsulated in the cylindrical metal container to be a statistically homogeneous continuum. An explosive pad, placed circumferentially as shown in Figure 1 is detonated parallel to the major axis of the cylinder using a lens arrangement placed at the top of the upper plug. On initiation, the detonation wave propagates parallel to the axis (Figure 2a) and the rarefaction wave generated at the free surface of the explosive pad propagates towards the axis of the cylinder (Figure 2b) and the explosion induces a shock into the powder. A reflection wave is introduced into the gaseous explosive at the explosive-powder interface (Figure 2b). Both the shock and the reflection waves are assumed to be radial in the model. The particle velocity and the pressure associated with the shock wave can be determined using impedance matching technique, where the particle velocity and the pressure are considered continuous across the powder-explosive interface. The shock thus introduced at the interface propagates into the powder aggregate radially, densifying the powder. The compressive wave reflected from the interface propagates radially outwards and on meeting the incoming rarefaction wave, vanishes as shown in Figure 2c. Finally the pressure in the compact reduces to zero when the rarefaction wave releases the shock in the compact as shown in Figure 2d.

High loading rate associated with a shock pulse causes temperature to rise, sometimes, even to the order of the melting point of the material. In this case if the pressure at the surface of the container is less than the required pressure for uniform compaction, we get compacts of lesser density due to under compaction and if the pressure is more, we may again end up getting low density compacts apparently due to melting and crack formation at the core of the cylinder. In an ideal condition, with a suitable explosive of optimum pad thickness, we get uniform compacts. The model focuses on the determination of various parameters to calculate the ideal condition.

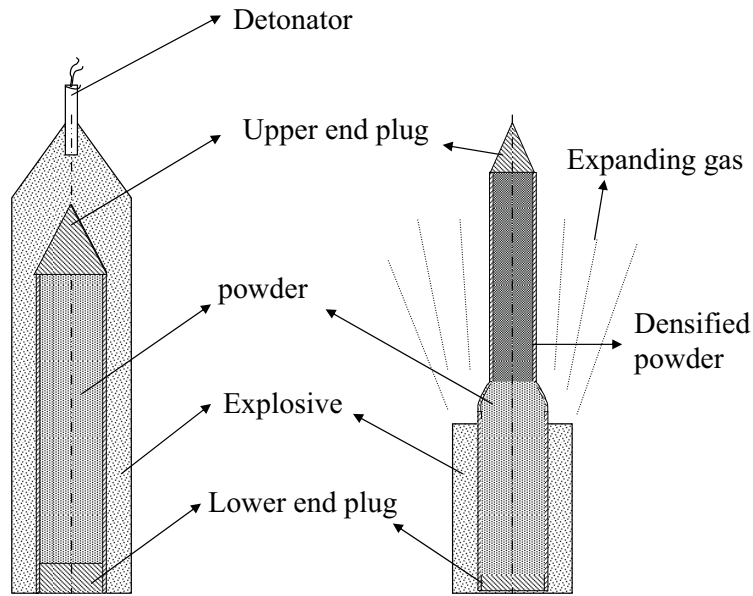


Figure 1: Schematic diagram of explosive compaction

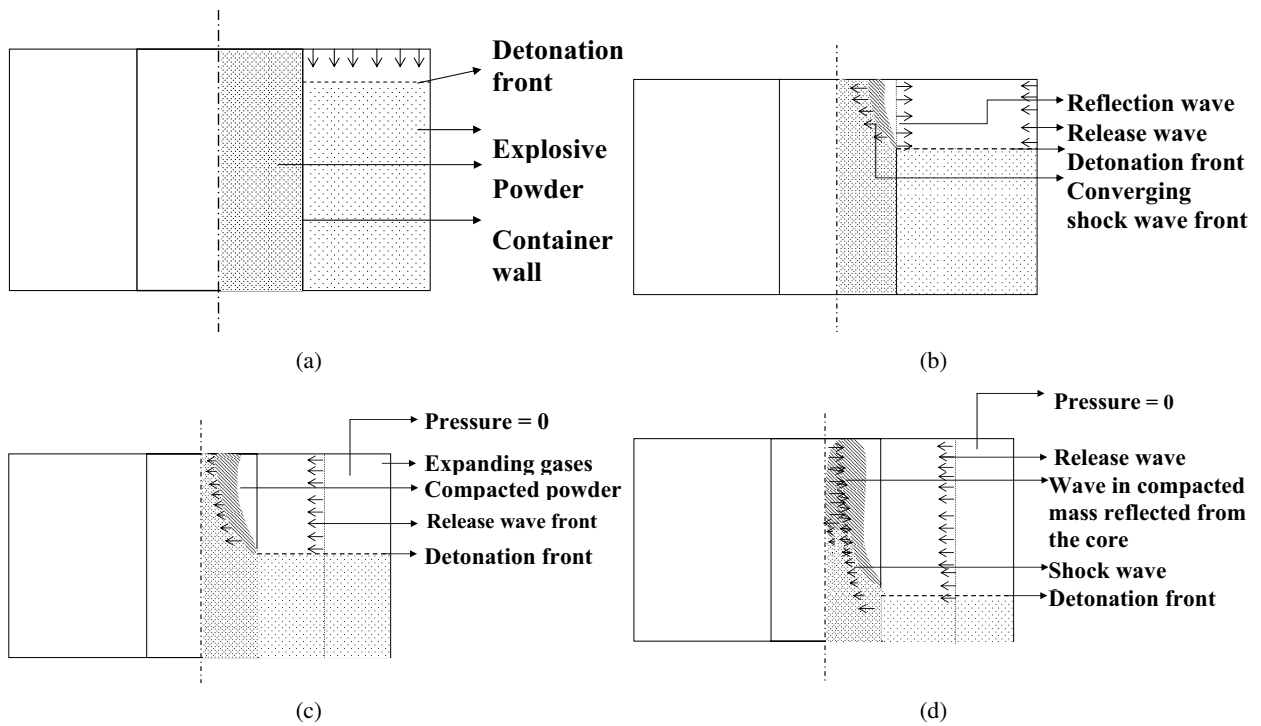


Figure 2: Schematic diagram of the model

2.1 Calculation of the pressure and the particle velocity at the explosive-powder interface using impedance matching technique

The Rankine-Hugoniot equations for conservation of mass and momentum are given by

$$\rho_{si}(U - u_i) = \rho_{sf}(U - u_f) \quad (1)$$

$$P_f - P_i = \rho_{si}(U - u_i)(u_f - u_i) \quad (2)$$

where U is shock wave velocity, u is particle velocity, P is pressure and ρ is density; the subscripts 'si' and 'sf' denote the values of these variables before and after the passage of the shock wave respectively.

The equation of state of the gaseous explosive for adiabatic condition is

$$P(1/\rho)^\gamma = \text{constant} \quad (3)$$

where γ is adiabatic constant, eliminating U , ρ_f from equations (1), (2) and (3) and assuming Chapman-Jouguet initial conditions, we get

$$(u_f - u_j)^2 = \frac{P_j}{\rho_j} \left[\frac{P_f}{P_j} - 1 \right] \left[1 - \left(\frac{P_j}{P_f} \right)^{\frac{1}{\gamma}} \right] \quad (4)$$

where subscript 'j' corresponds to Chapman-Jouguet condition.

The shock velocity in porous materials (Ramakrishnan, 1988) is given by

$$U_\theta = \psi_\theta C_\theta + g_\theta u_i \quad (5)$$

where u_i is the initial particle velocity. The pore collapse function ψ_θ , material parameter g_θ and the effective bulk sound speed C_θ are

$$\psi_\theta = \left[\frac{\sqrt{3}u_i}{C_\theta} \right]^{1.5\theta};$$

$$g_\theta = \left[\frac{g_\theta}{1 + \theta(g - 1)} \right];$$

$$C_\theta = C \sqrt{\left[\frac{1 - \theta}{1 + b_K \theta} \right]}$$

where $C = \sqrt{\frac{K}{\rho_0}}$, $b_K = \frac{1+\nu}{2(1-2\nu)}$ and the porosity $\theta = 1 - \frac{\rho_{si}}{\rho_0}$. ρ_{si} is the initial density of the powder or the partially densified material as the case may

be just before the shock wave entering into the medium. It has to be appropriately substituted in these equations. For example, in the case of reflected shock wave through partially densified material, the initial porosity refers to the porosity of the material prior to a shock propagation in this medium and is valid only for $\theta > 0$. The subscript θ corresponds to the effective porous material with porosity θ . Effective porosity is the porosity of powder/partially-densified material. K is the bulk modulus; ρ_0 is the density of the powder material with zero porosity. ν is the Poisson's ratio, and g is a material parameter for dense material that appears in the linear equation of the state. Therefore the pressure generated by the shock in the powder material is

$$P = \rho_0(1 - \theta)u_i U_\theta \quad (6)$$

Equations (4) and (6) essentially relate the pressure and the particle velocity in the explosive and the powder material, which are continuous across the interface.

2.2 Speeds of reflection and rarefaction waves in explosive

Using Equation (3) in the gaseous explosive for adiabatic conditions, the speed of the reflection and the rarefaction wave to be,

$$a = \sqrt{\frac{dP}{d\rho}} = \sqrt{\frac{\gamma P_j}{\rho_j} \left(\frac{\rho_e}{\rho_j} \right)^{\gamma-1}} \quad (7)$$

where P_j and ρ_j are Chapman-Jouguet pressure and density respectively; ρ_e is the density of the gaseous form of the explosive. The density of the explosive in this medium from Equation (3) is given by

$$\rho_e = \rho_j \left(\frac{P}{P_j} \right)^{\frac{1}{\gamma}} \quad (8)$$

where P is the pressure at the interface. For Chapman-Jouguet state i.e. when $\rho_e = \rho_j$ the Equation (7) reduces to

$$a_j = \sqrt{\frac{\gamma P_j}{\rho_j}} \quad (9)$$

Equation (9) is the speed of the rarefaction wave at the free surface propagating towards the axis and the reflection wave generated at the interface moving towards the outer surface. Speeds being nearly equal these are assumed to intersect at the mid-point of the explosive pad. This reflection wave weakens with the incoming rarefaction wave moving finally towards the centre of the cylinder with a speed given by Equation (9).

2.3 Calculation of the intersection point and the distance of the rarefaction wave and the shock wave in the powder

In the gaseous explosive, the reflection and the rarefaction waves are assumed to be moving with the same speed but in the opposite directions meeting each other at the mid point of the explosive pad because pressure-volume state is same for both the cases as shown in Figure 2(b). Then this rarefaction wave moves towards the centre of the cylinder through the compacted dense material as shown in the Figure 2(c). The rarefaction wave intersects with the preceding shock wave in the powder, which is propagating towards the center of the cylinder. This rarefaction wave releases the shock in the powder compact. Depending on the thickness of the compact and the wave speed, the rarefaction wave may catch-up with the shock wave before it reaches the center of the cylinder, in which case, the rod end-up under-compacted. This happens when the pressure is applied for insufficient duration on the porous material, which is related to the insufficient explosive pad thickness. On the other hand the rods are over-compacted leading to melting at the core, when there is enough time for the unloading shock wave to get reflected at the core. This reflection wave meets the release wave, apparently, which also results in lower density, because of melting due to the high pressure at the core. Ideally, the rods will be of uniform density if the release wave meets the shock wave exactly at the central axis of the cylinder and terminates the shock compression.

The densification of the compact due to shock loading is obtained using Equation (1). The density of the compact due to unloading decreases

when the rarefaction wave sweeps through the radius. The final density is calculated using Equations (1) and (2) and by substituting $P_f = 0$ in Equation (2). A detailed algorithm for the numerical computations is presented in the form of a flow diagram shown in Figure 3.

3 Densification due to melting

This part of the model describes the temperature distribution in the shock induced dynamically compacted powder particles. This model is a modified form of that by Gourdin (1984). As shown in Figure (4), the powder is subjected to a shock wave and a fraction of the dissipation energy is deposited at the interface between the powder particles. As observed experimentally by Gourdin (1984), a uniform energy deposition at the particle surface is assumed and the net energy deposited at the surface of the powder particles during compaction is expressed in terms of the energy deposited per unit mass. Heat transfer equation is employed to get the temperature variation from the surface to the center of the powder particle. The model includes the effect of latent heat also.

The specific energy carried by the shock is given by the Rankine-Hugoniot relation

$$E_f - E_i = (P_f + P_i)(V_i - V_f)/2 \quad (10)$$

where E , P and V are energy, pressure and specific volume respectively and the subscripts 'i' and 'f' refer to the initial and final states. The net energy deposited on the surface of the particle is assumed to be 90% of the area under the pressure-volume curve of the material. The inter-particle bonding in dynamically compacted materials is a result of localized melting at the interfaces. It is assumed that the net shock energy deposited at the particle interface is uniform (Raybould, 1980; Raybould, 1981; Gourdin, 1984) as shown schematically in Figure 4, where ω is the thickness of the surface layer up-to which the deposited energy is conducted and ω^* is the thickness of the surface layer which gets melted.

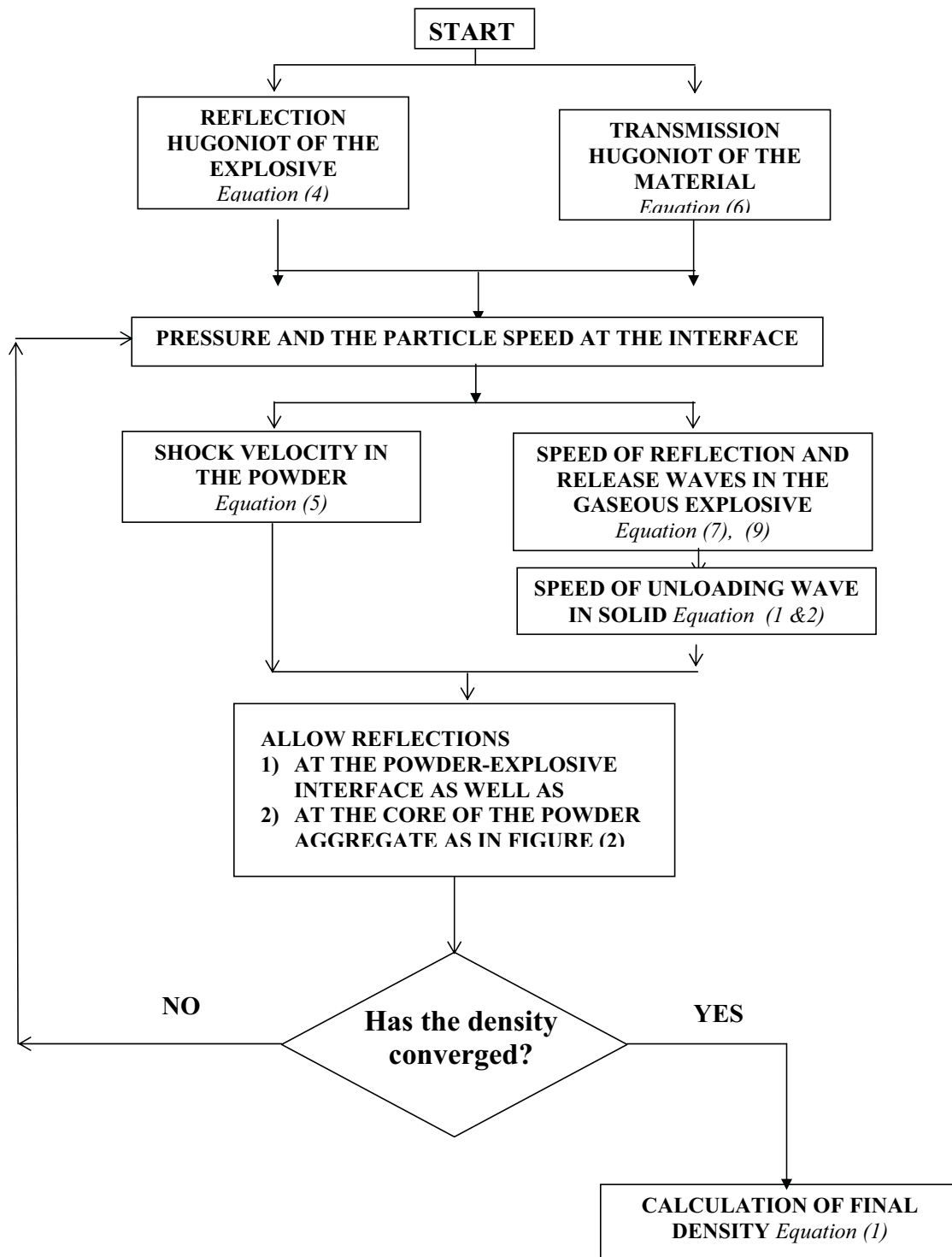


Figure 3: Flow diagram to compute the densification during explosive loading

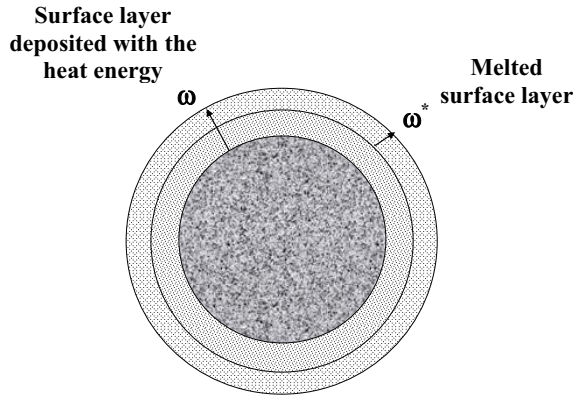


Figure 4: Model of the energy deposition on the powder surface

3.1 Calculation of Temperature distribution

Let ρ_{ti} and ρ_{tf} be the initial and final densities of the powder corresponding to before and after melting. Therefore

$$\rho_{ti} = \frac{1}{V_0 + V_\theta} \quad (11)$$

where V is the volume per unit mass. The subscript '0' and ' θ ' correspond to dense and porous states respectively. Here, the porous state corresponds to that prevailing after the shock loading (i.e. $\rho_{ti} = \rho_{sf}$)

$$\rho_{tf} = \frac{1}{V_0 + V_\theta - \Delta V_\theta} \quad (12)$$

where ΔV_θ is the volume of the melted powder that contributes to the densification of the compact due to melting alone. If $V_\theta < \Delta V_\theta$ then naturally it has to be reset as $\Delta V_\theta = V_\theta$.

Subtracting Equation (11) from Equation (12) and using Equation (11) we get

$$\rho_{tf} - \rho_{ti} = \frac{1}{V_0 + V_\theta - \Delta V_\theta} - \frac{1}{V_0 + V_\theta} \quad (13)$$

$$\Delta \rho_t = \frac{\Delta V_\theta \rho_{ti}^2}{(1 - \rho_{ti} \Delta V_\theta)} \quad (14)$$

It is assumed that from each particle the volume that melts at the surface goes into the pores to the

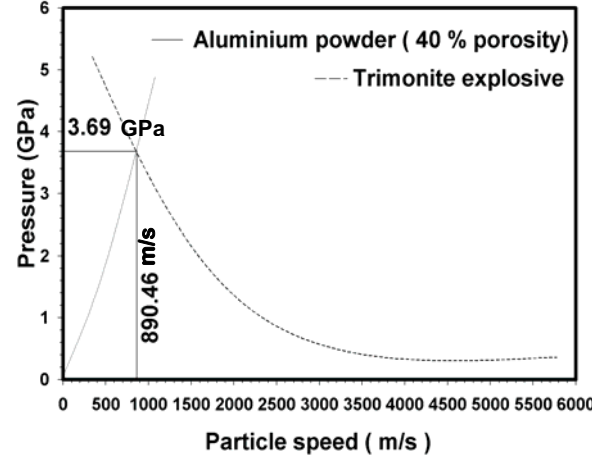


Figure 5: Pressure-particle relationships for Aluminium and Trimonite Explosive and determination of the interface pressure and the speed

extent that it does not exceed the available pore volume. The volume of the melted portion of the particle that fills the pore is given by $4\pi r^2 \omega^*$, where r is the radius of the powder particle and ω^* is thickness of the surface layer, which gets melted.

Therefore the volume which fills the pores per unit mass is

$$\begin{aligned} \Delta V_\theta &= 4\pi r^2 \omega^* \times \frac{3}{4\pi r^3 \rho_0} \\ &= \frac{3\omega^*}{r\rho_0} \quad \text{for } V_\theta > \Delta V_\theta \\ &= V_\theta \quad \text{for } V_\theta < \Delta V_\theta \end{aligned} \quad (15)$$

Let c_v be the specific heat at constant volume, ω be the thickness of the surface layer through which the deposited heat has been conducted and K is the thermal conductivity of the material. T_m and T_r are the melting and room temperatures of the material. Let T_f be the maximum temperature that is developed on the surface of the material. Using the steady state thermal conductivity equation, the heat flux through the surface of the powder particle is given by

$$\frac{k4\pi r^2(T_f - T_r)}{\omega} = \frac{k4\pi r^2(T_f - T_m)}{\omega^*} \quad (16)$$

The above equation assumes uniform conduction through only a thin layer on the surface. From the

above equation we get

$$\omega^* = \omega \left(1 - \frac{T_m - T_r}{T_f - T_r} \right) \quad (17)$$

Equating the energy deposited on the surface of the particle in time 't' to flux rate we get

$$\frac{k4\pi r^2(T_f - T_r)}{\omega} = \frac{\alpha\eta 4\pi r^3\rho_0}{3t} \quad (18)$$

where α is a fraction less than one and η is the energy deposited on the particle surface as given by Equation (10).

$$\eta = \frac{1}{2}P\Delta V \quad (19)$$

where P is the maximum pressure and ΔV is the change in powder volume per unit mass of the powder and t' is the time taken by the shock wave to travel through the diameter of one particle in the effective porous medium; it is given by

$$t = \frac{2r}{(1-\theta)U_\theta} \quad (20)$$

Substituting Equations (19) and (20) in Equation (18) we get

$$T_f - T_r = \xi \omega \quad (21)$$

where

$$\xi = \frac{\alpha P(\Delta V)\rho_0 U_\theta (1-\theta)}{12K} \quad (22)$$

The porosity ' θ ' here corresponds to the porosity at the end of the shock loading. The heat deposited on the surface of the powder particles of unit mass is

$$\begin{aligned} \rho_0 \omega 4\pi r^2 c_v (T_f - T_r) + \rho_0 \omega^* 4\pi r^2 L \\ = \frac{1}{2} P(\Delta V) \alpha \frac{4}{3} \pi r^3 \rho_0 \end{aligned} \quad (23)$$

where ' L ' is the latent heat of the melting powder material.

On simplifying the above equation we get,

$$\rho_0 \omega c_v (T_f - T_r) + \rho_0 \omega^* L = \xi \frac{2Kr}{(1-\theta)U_\theta} \quad (24)$$

Using Equations (17) and (21) in Equation (23) we get

$$\begin{aligned} \omega^2 + \left(\frac{L}{c_v \xi} \right) \omega \\ - \left[\frac{L(T_m - T_r)}{c_v \xi^2} + \left(\frac{2rK}{(1-\theta)c_v \rho_0 U_\theta} \right) \right] = 0 \end{aligned} \quad (25)$$

On solving the above quadratic equation in ω we get

$$\begin{aligned} \omega = -\frac{1}{2} \frac{L}{c_v \xi} \\ + \frac{1}{2} \sqrt{\frac{L^2}{c_v^2 \xi^2} + 4 \left[\frac{L(T_m - T_r)}{c_v^2 \xi^2} + \frac{2rK}{(1-\theta)\rho_0 U_\theta c_v} \right]} \end{aligned} \quad (26)$$

The final density ρ_f is calculated using Equation (13) along with Equations (14), (15), (17), (21) and (25).

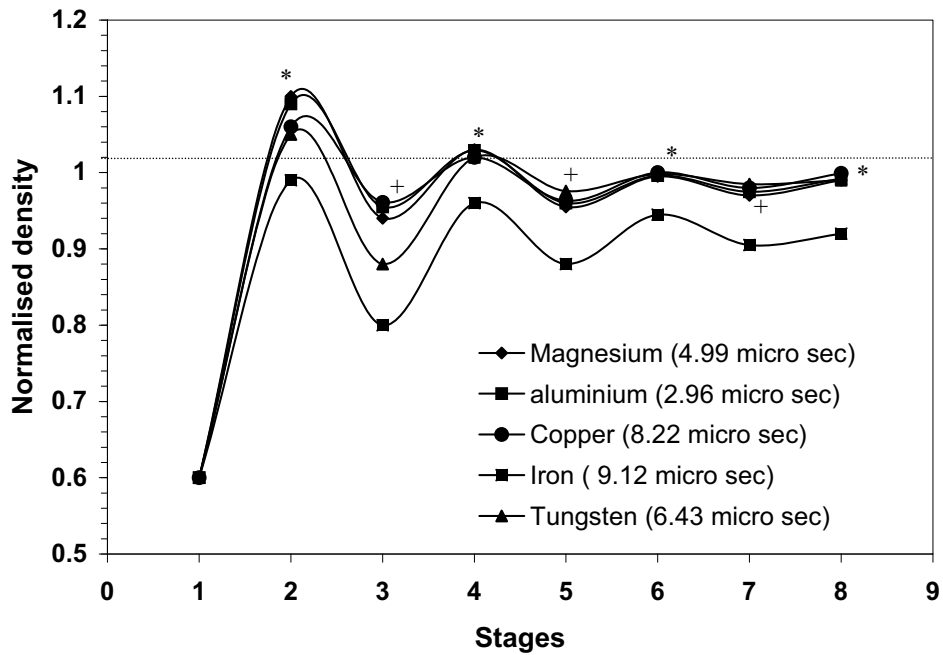
4 Results

4.1 Validation

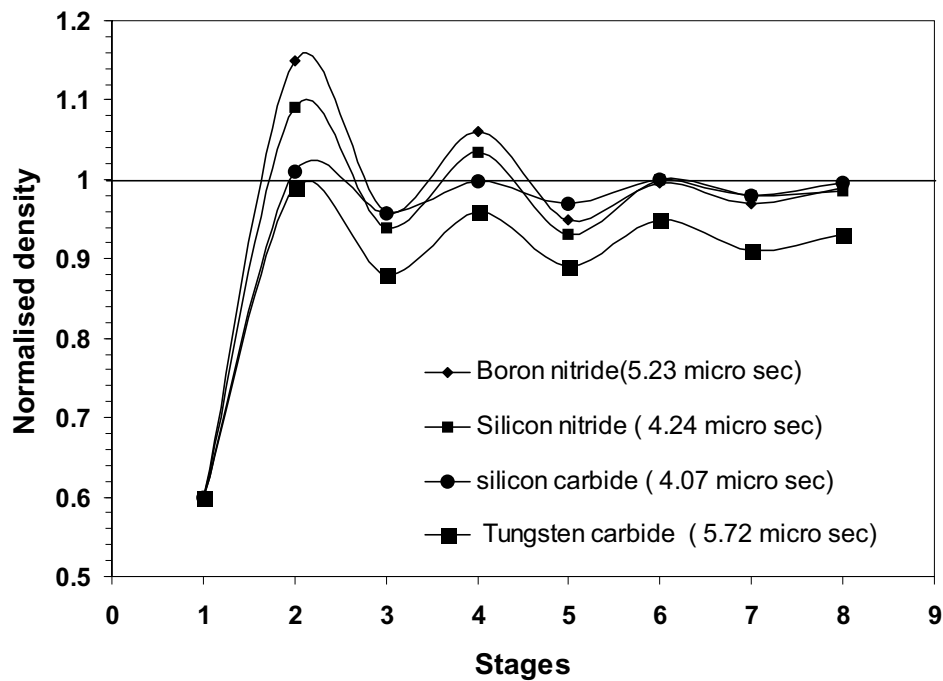
In this model, a cylindrical container of diameter 16mm and height 60mm is filled with different types of powders (listed in Table 1) that measures to ~40% porosity. For this investigation trimonite explosive is considered as an illustrative explosive material for calculations, same as in the experimental work carried out by Siva Kumar (1996) for compaction of aluminium powder. The density of this explosive is 1080 kg/m³. Detonation velocity and Chapman-Jouguet pressure of the explosive are 4300 m/s and 7.11 GPa respectively (Siva Kumar; 1996). The explosive pad of thickness varying from 1mm to 25mm is mantled to this cylinder to study the effect of pad thickness on compact densities so as to find the ideal pad thickness for a given material.

The model takes into account the effect of particle size also on densification as discussed in section 3. But in this paper, the discussions are restricted to the optimum size of the particle and ideal pad thickness of the explosive pad. The graphs plotted in Figures (6) and (7) correspond to optimum size of the particle and ideal thickness of the explosive

Explosive: Trimonite
 Initial Diameter of the powder agglomerate: 16 mm
 Initial porosity: 40 %



(a)



(b)

Figure 6: Progressive densification for different materials during explosive compaction

Table 1: Material properties (Metals reference; 1993)

Powder Material	Density (Kg/m ³)	Young's Modulus (GPa)	Poisson's ratio	Thermal conductivity (W/m.K)	Melting/softening temperature (K)	Specific heat (J/Kg.K)	Compression factor g	Bulk sound speed C ₀ (m/sec)	Latent heat (J/Kg) (X10 ⁴)
Mg	1740	44	0.29	157.3	923.2	1046	1.263	4492	44
Al	2785	69	0.29	205	933.25	913	1.338	5328	38
Cu	8930	119.5	0.3	380.8	1356.15	385	1.489	3940	21.17
Iron	7850	115	0.27	47.71	1373	497.9	1.92	3574	9.63
W	19400	390	0.3	200.8	3653	125.5	1.237	4029	65
BN	2270	176	0.25	6.97	3000	730	1.0	6530	122.6
Si ₃ N ₄	3310	311	0.27	7	2173	740	1.0	8000	125
SiC	3120	400	0.27	60	2473	670	0.95	8000	183.52
WC	15800	669	0.25	25.3	2900	740	1.339	4920	70

Explosive material	Density (Kg/m ³)	Detonation Velocity (m/sec)	Energy (KJ/Kg)	γ	Chapmann-Jouguet Pressure (GPa)	Chapmann-Jouguet Density (Kg/m ³)
Trimonite	1100.0	4300	5500	1.64	7.01	2000

pad. The effect of particle size on densification will be discussed more elaborately in our next paper (Srivathsa and Ramakrishnan). The 'depth of densification' in our study refers to the thickness of the cylinder up to which the densification has taken place; in other words, it is the distance at which the shock pressure is annulled by the release wave.

The model is validated for final compaction density as well as the surface temperature and the melted surface thickness of the powder particle with the available experimental results. The computed optimum pad thickness of trimonite explosive for compaction of aluminium powder with 40 % porosity is ~ 5 mm as shown in Figure (8), which is in good agreement with experimental results of Siva Kumar (1996). Further, micro structural studies carried-out by Siva Kumar (1996) with varying pad thickness reveal that pad thickness less than 5 mm results in under-compaction at the core and above that causes melting at the core, which is in line with the model prediction. The computed surface temperature of the

aluminium particle is 951 °K, where the melting point of aluminium is ~ 933 °K, that is marginally higher than its melting temperature at the atmospheric pressure. Therefore, the contribution for densification due to melting can't be significant because the thickness at the particle surface that is melted is very small as shown in Figure (7). The computed thickness of the aluminium particle that is melted due to high temperature is ~ 0.25 mm, which is also in agreement with experimental results of Lotrich (1986). The computed surface temperature and the melted surface thickness of the copper particle are compared with the experimental results of Gourdin (1984) and Bergmann (1973). Unlike aluminium, the contribution for densification due to melting in copper is very significant. The computed surface temperature of copper particle is 1415 °K, where the melting point of copper is ~ 1356 °K, which is significantly higher than its melting temperature. Also the conductivity of copper is higher than the conductivity of aluminium. Similarly the specific heat of copper is less than the specific heat of aluminium; therefore the contribution for densi-

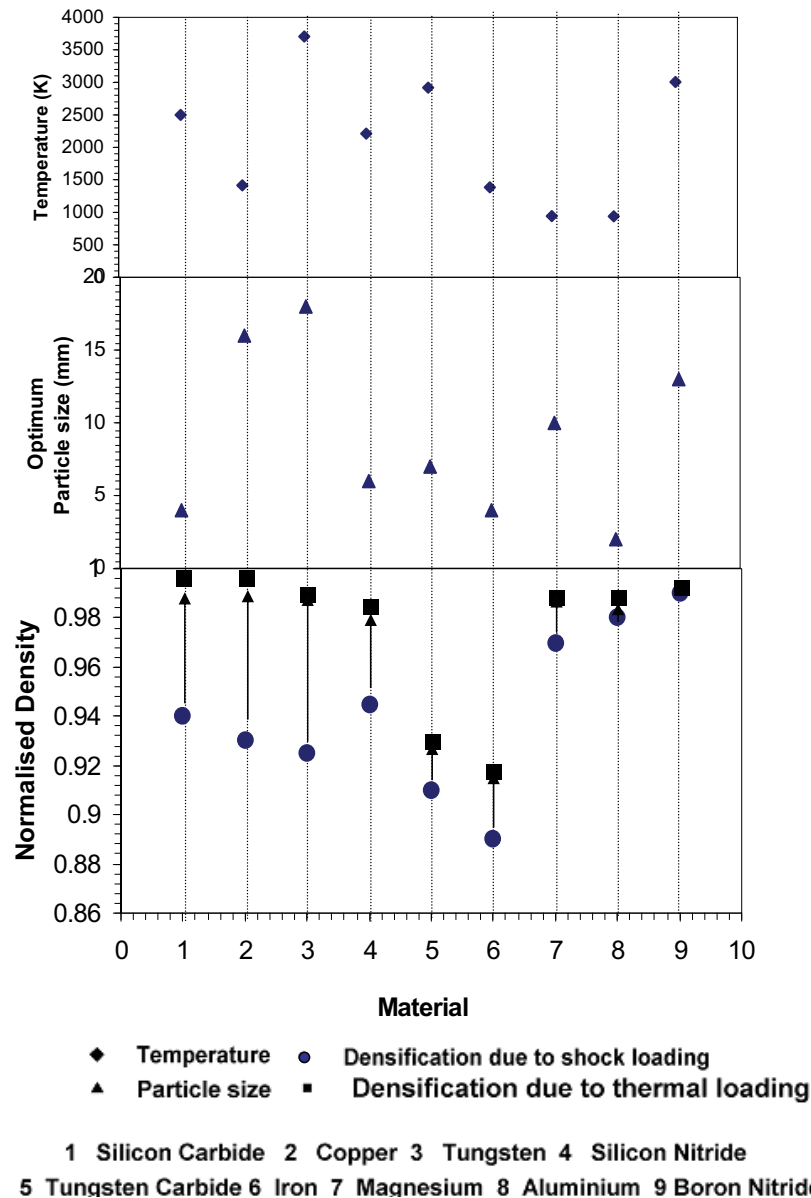


Figure 7: Effect of particle size on the densification and temperature at the surface of the powder particles for different materials

fication due to melting should be high for copper. This is also reflected by the surface thickness melted on copper particle, which is ~ 0.7 mm. These values are in good agreement with the experimental results of Gourdin (1984) and Bergmann (1973).

4.2 Discussions

The interface pressure and the particle velocity are independent of the explosive pad thickness,

but depend on the characteristics of the powder as well as the explosive material. As an illustration, the pressure and the particle velocity at the aluminium powder-explosive interface is shown in Figure (5). These curves are obtained from Equation (4) that is a well-known reflection Hugoniot relation. Equation (6) relates the pressure and the particle velocity in a porous medium (Ramakrishnan; 1988). The pressure and the particle velocity at the interface of the aluminium powder that measures to 40% porosity and the trimonite ex-

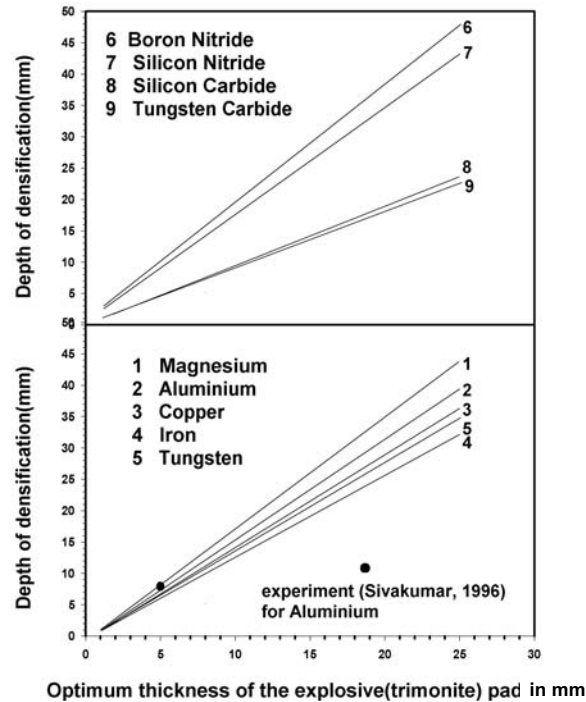


Figure 8: Effect of pad thickness on densification

plosive are ~ 3.7 GPa and 900 m/s respectively.

The computed final density due to shock as well as thermal loading for different metallic materials is shown in Figure 6(a) and for ceramics in Figure 6(b). The diameter of the powder agglomerate is taken as 16 mm and the thickness of the explosive pad used for optimum densification is different for different materials. The positions of crests (*) shown in Figure 6(a) denote the densities obtained by compression wave originated from the interface and the positions of troughs (+) denote the densities realized by the release wave originating from the center of the cylinder. It can be observed that, with the initial shock wave itself the density of the compacts of these powders exceeds the original density (except tungsten) subsequently the release wave relaxes the material, reaching the positions of troughs below the base density, but to a density higher than the initial density (i.e. $0.6\rho_0$). This process continues till the pressure becomes zero that is the rarefaction wave approaching the center of the cylinder attenuating the shock wave. Figure 6(b) the convergence effect and also the propagation of the

shock, reflection as well as rarefaction and release wave phenomena explicitly. Figure 6 specially corresponds to the optimum pad thickness and specific particle size. The convergences shown for each material is different for different particle size and also pad thicknesses. Therefore, the time required for convergence is also different, which are shown within brackets in Figure 6(a). For example, the optimum particle size for magnesium powder is $10 \mu\text{m}$ (Figure 7) and the optimum explosive pad thickness is ~ 4.5 mm (Figure 8). The optimum particle size and optimum explosive pad thickness for ideal compaction are shown separately in Figures (7) and (8). From Figure 6(a) it can be observed that low to moderate density materials converge to a higher theoretical density, whereas higher density material like tungsten converges to a lower theoretical density. It is also clear that low-density materials densify with greater speed compared to moderate density materials. One of the reasons to this variation is low specific heat of the material in addition to its bulk density. And also lower compression factor of tungsten can be attributed to low compacted density. Never the less, the change in explosive material will change the optimum parameters. It is this nature of the explosive compaction makes this modelling highly relevant.

Similar trend, as seen in metallic materials, is observed in ceramic materials also. In the set of composites considered in this study, Low-density ceramics densify faster than that of the high-density ones. The convergence time for densification of boron nitride is marginally high compared to the other low-density ceramics. Boron Nitride converges very close to original density and the time to converge is marginally high unlike metallic powders. Otherwise, higher density ceramics Tungsten Carbide is falling in line with that of metallic powders. The variations in densification of these ceramics are attributed to the complex combination of bulk sound speed, thermal conductivity, latent heat, specific heat capacity and compression factor etc.

Figure 7 provides a broader idea of the model in terms of the effect of the particle size, surface temperature of the particle on densification due to

shock loading as well as thermal loading. This figure consists of three plots; i) the density obtained due to shock and thermal loading, ii) the optimum particle size and iii) the temperature developed at the surface of the particle. The percentage contribution due to the combined effect of the shock loading as well as the melting for different materials using optimum pad thickness is shown in Figure 7. The overall densification is close to 99% for almost all materials listed in Figure 7, except Tungsten Carbide and Iron. Interestingly, it can be observed that among the materials listed the contribution to densification due to melting is significant in Silicon Carbide, Copper, Tungsten and Silicon Nitride. It is moderate in Tungsten Carbide, Iron and Magnesium. In the case of Boron Nitride and Aluminium it is negligible. For the given explosive material and the other parameters naturally for the materials for which the temperature attained is significantly higher than their respective melting or softening temperature, the thermally induced densification turns out to be higher. Second plot of Figure 7 contains the optimum particle size. The optimum size of the powder particle is below $6\ \mu\text{m}$ for silicon carbide, silicon nitride, Iron and aluminium. In case of the tungsten carbide and magnesium the optimum size fall in the range of $6\ \mu\text{m} - 14\ \mu\text{m}$, and larger in the case of Boron nitride, copper and tungsten. Figure 8 shows the effect of the explosive pad thickness and the depth of densification. The depth of densification in our study refers to the radial thickness to which the densification has taken place; in other words, it is the distance at which the shock pressure is nullified by the release wave. It can be observed that for a given pad thickness, the depth of densification is high for low-density materials. This graph also throws light on ideal pad thickness to achieve maximum densification. For instance, in the case of Boron Nitride if the radius of the cylindrical container is $\sim 10\text{mm}$, the optimum trimonite explosive pad thickness is around 6mm . Interestingly, the depth of densification varies linearly with the explosive pad thickness as per the model.

5 Summary

The paper describes an analytical model of an explosive compaction of powder with axial detonation to obtain cylindrical billets. The model mainly focuses on two important design parameters: i) the explosive pad thickness ii) particle size. The effect of number of mechanical and thermal properties of the powder as well as the properties of the explosive material is incorporated in the model. Shock dynamics is used for arriving at the optimum explosive pad thickness. The shock energy deposition at the particle surface is used for determining the temperature distribution and melting leading to optimum particle size. Although, only a few illustrative cases have been presented in this paper, the model has a wider applicability.

Acknowledgement: The authors thank the Director, DMRL, for his encouragement and for permission to publish this paper and Dr. Siva Kumar for useful discussions.

References

- Benson, David J.; Nellis, W. J.** (1994): Dynamics compaction of copper powder: computation and experiment, *Appl. Phys. Lett*, 65(4), 199.
- Bergmann, O. R.; Barrington, J.** (1965): Effect of explosive shock waves on powders, *Jl. of the American ceramic society*, 49(9), 502-507.
- Bogdanov, A. P.** (1969): Compacting of metal powders by high explosives, *Powder metallurgy*, 12(24), 613-620.
- Byvshikh, A. I.; Kirko, V. I.; Pak, N. I.** (1991): Modeling thermal processes in the shock loading of porous materials, *Journal of Applied Mechanics and Technical Physics*, 32(4), 592-596.
- Carlson, R. J.; Porembka, S. W.; Simons, C. C.** (1966): Explosive compaction of ceramic materials, *Ceramic bulletin*, 45(3), 266-270.
- Gohl, B. W.; David, A. Ward** (2000): Application of explosive compaction for tailing volume reduction, *Geotechnique*, 38, 435.
- Gourdin, W. H.** (1984): Energy deposition and microstructural modification in dynamically con-

solidated metal powders, *Jl. of App Phy*, 55(1), 172-181.

Grover, R.; Urtiew, P. A. (1974): Thermal relaxation at interface following shock compression, *Jl. of App Phy*, 45 (11), 146-152.

James, P. J. (1972): Fundamental aspects of the consolidation of powders, *Powder Meta. Intl.*, 82, 145-197.

Lee, Y. K. (1985): Specific surface area studies of shock-modified inorganic powders, *Jl. of Material Science*, 20, 2488-2496.

Lennon, C. R. A; Bhalla, A. K.; Williams, J. D. (1978): Explosive compaction of metal powders, *Powder metallurgy*, 1, 29-34.

Li, Shujie; Khosrovabade, Paul B.; Kolster, Ben H. (1994): New compaction equation for powder materials, *Intl. Jl. of powder metallurgy*, 30(1), 47-57.

Liu, Ht.; Han, Z. D.; Rajendran, A. M.; Atluri, S. N. (2006): Computational modeling of impact response with the RG damage model and meshless local petrov-Galerkin approaches, *CMC: Computers, Materials and Continua*, 4(1), 43-53.

Maksimenko, L. A.; Maksimenko, A. L.; Serdyuk, G. G.; Shtern, M. B. (1991): hock waves in dynamic compacting powders and porous bodies, *Poroshkovaya metallurigiya*, 9(345), 15-19.

National Material Advisory Board (1983): Dynamic compaction of metal and ceramic powder report no. MDA-903-82-c-0434.

Prümmer, R. A. (1973): Latest results in the explosive compaction of metal & ceramic powders and their mixtures, *IV Intl. Conf. on the center for high energy forming*, 9-13.

Prümmer, R. A. (2004): Explosive Compaction of powders, principle and prospects, *Materialwissenschaft und werkstofftechnik*, 20(12), 410-415.

Rajendran, A. M.; Grone, D. J. (2003): Computational modelling of shock and impact response of alumina, *CMES: Computer Modelling in Engineering and Science*, 3 (3), 367-380.

Ramakrishnan, N.; Siva, Kumar K. (1988): An equation of state for porous materials under shock

loading, *Bull of material Science*, 11(1), 75-85.

Raybould, D. (1980): The cold welding of powders by dynamic compaction, *Intl. Jl. of Powder metallurgy & powder technology*, 16(1), 9-19.

Raybould, D. (1981): The production of strong parts and Non-equilibrium Alloys by dynamic compaction, in shock waves and High-strain-rate phenomena in metals, edited by M.A. Meyers and L.E. Murr (Plenum, New York).

Roshan, kumar D.; Krishna, Kumar R.; Phillip, P. K. (1999): Simulation of dynamic compaction of metal powders, *Jl. of App Phy*, 85 (2), 1-9.

Schwartz, R. B.; Kasiraj, T.; Vreelan, T.; Ahrens, T. J. (1984): Temperature kinetics during shock-wave consolidation of metallic powders, *Acta metall*, 32 (8), 1243-1252.

Siva, Kumar K. (1996): Studies on explosively compacted Aluminium matrix silicon carbide particulate composites, *Ph. D. thesis*, I.I.T Mumbai, India.

Smithells (1993): ASM Metals reference book, 3rd ed., Materials Information society, Ohio, USA.

Srivathsa, B.; Ramakrishnan, N.: A parametric analysis of axially detonated explosive compaction of cylindrical billets, to be published.

US Energy & Research Development Proj. No. W-7405, *Hydrodynamic modelling and explosive compaction of ceramics*, Lawrence Livermore Laboratory, Livermore, California, -Eng-48.

Victor, F. Lotrich; Tamotsu, Akashi; Akira, Sawaoka (1986): A model describing the inhomogeneous temperature distribution during dynamic compaction of ceramic powders, *Metallurgical applications of shock wave & high-strain-rate phenomenon*, Edited by L.E.Murr, K.P. Staudhammer and Marc A Meyer, Publishers Marcel Dekker Inc.

Yukio, Sano (1977): A continuum approach to dynamic compaction of metal powder, *Intl. Jl. of powder metallurgy & powder technology*, 3(2), 81-98.

